77th IIW Annual Assembly and International Conference on Welding and Joining 7-12 July 2024 Rhodes, Greece

On the influence of process parameters on the dimensional accuracy and microstructure of wire electron beam additive manufactured Ti-6Al-4V alloy

Frederic Wilhelm Schlieker[1*], *Dzhem Kurtulan*[1], and *Ghazal Moeini*[1]

[1]Institute of Mechanical Engineering, Westphalian University of Applied Sciences, Gelsenkirchen, Germany

Abstract. Directed Energy Deposition-Electron Beam (DED-EB) stands out as a cost-competitive and efficient additive manufacturing process for fabricating large and intricate components from highly reactive materials. This study delves into the DED-EB process applied to a Ti6Al4V alloy, exploring the impact of several critical process parameters, namely welding velocity, electron beam oscillation, and wire feed direction, on geometrical accuracy, microstructure, and resultant mechanical properties. The investigation reveals that welding velocity and wire feed direction significantly affect the volume and geometrical accuracy of the specimens, whereas the influence of electron beam oscillation on these parameters remains minimal. Notably, the results demonstrate that at the utilized slow welding velocities, the wire feed direction significantly influences the microstructure by mitigating columnar grain growth in the fabricated structures. Additionally, it is observed that more complex oscillation patterns appear to impact the development of columnar grain growth.

1 Introduction

Over time, various additive manufacturing processes have matured into a competitive alternative to conventional production in many areas. In metal fabrication, the feedstock can be categorized into wire-based and powder-based processes [1]. While powder-based processes achieve high accuracy and good surface quality, they are limited in deposition rate due to the micrometer-scale powder grains used. Furthermore, powder-based processes are constrained by the dimensions of the process chamber. In contrast, wire-based processes enable a significantly higher deposition rate with lower geometrical accuracy and surface quality. This lower accuracy often necessitates subsequent subtractive processing [2-7]. There are many possible energy sources for the additive manufacturing process, such as arc, laser beam, or electron beam. Especially for processing reactive or high melting alloys an electron beam as power source is advantageous [8-11]. So, for the fabrication of reactive metals like titanium and its alloys, the usage of DED-EB is a useful choice to avoid any reactions with atmospheric gases during the fabrication process [10-14]. The commercial most important titanium alloy nowadays is Ti6Al4V for its meaning for biomedical and aerospace industries [13,15]. Ti6Al4V is a titanium alloy of α+β configuration which consists mainly of hexagonal α - titanium as well as body-centered cubic β-titanium. Its properties depend on the segregation of elements, defects, and microstructure [16]. Those characteristics are highly influenced by the cyclic thermal load of the additive manufacturing process whose effects are similar cyclic heat treatment. This treatment leads to an anisotropic material behavior triggered by columnar growth of prior β-grains and expansion of lamellar α-phase [15,17]. Various technological input parameters can significantly influence the microstructural and mechanical properties of DED-EB processed components [18]. Previous studies have demonstrated that parameters such as beam current and welding speed affect the properties and dimensions of manufactured components [19]. Notably, the deposition strategy has a strong impact on the temperature distribution, which in turn affects the resulting mechanical behavior [20]. Another important process parameter for determining the distribution of the heat input during the formation of deposition layers is the electron beam oscillation [21]. This work considers the influence of different selected oscillation figures, welding speed, and wire feed directions on the geometrical accuracy, grain structure development, and micro-hardness of Ti6Al4V components processed by DED-EB.

2 Material and Methods

The used titanium alloy wire with the specification Ti6Al4V (Grade 5) was used in the commercially available diameter of 1.2 mm. It was applied on a substrate plates of Grade 5 titanium with a thickness of 8 mm. The chemical composition of wire and substrate were determined by energy dispersive X-ray spectroscopy by using a scanning electron microscope (Zeiss Sigma 300 VP, Oberkochen, Germany) the results are shown in Table 1 the measurement of the chemical composition is within the requirements of the materials specifications.

* Corresponding author: frederic.schlieker@w-hs.de

Table 1. Chemical composition (wt.%) of wire and substrate

Sample	Ti	Al	V	Fe
Ti6Al4V-Wire	89.3	6.3	4.2	0.2
Ti6Al4V-Substrate	89.6	6.2	4.0	0.2

All considered welding experiments were carried out using an electron beam welding machine EBW 700/6-60 CNC by PTR GmbH (PTR GmbH, Germany). The working chamber pressure was below $2{,}5\times10^{-2}$ mbar. The wire feed was realized by a drive unit DIX FD 101 LS-V and controlled by DIX FDE 100L both of DINSE GmbH (DINSE GmbH, Germany). All experiments were made with a stationary nozzle and a three-axis table to move the substrate. The nozzle was set to an angle of 45 degree relative to the substrate surface with 1 mm between the wire tip and substrate. During all experiments the acceleration voltage and used beam current were kept constant at 60 kV and 15 mA with a constant wire feed speed of 0.9 m/min. The power per volume ratio was constant at 53.05 W/mm³. The focus of the electron beam was set on the substrate surface. Three different oscillation figures with an outer diameter of 5 mm and increasing complexity were considered, they are shown in table 2.

Table 2. Overview of the used oscillation figures.

Oscillation figure	Circle	Square pulse	Distorted Infinity
Figure			

There were two different wire feed directions tested. One orthogonal to the main movement direction (side feeding) of the table and one within the main movement direction of the table (front-back feeding). A full overview of all parameters is listed in Table 3.

Table 3. Overview of the used process parameters.

Oscillation frequency	200 Hz		
Oscillation diameter	5 mm		
Acceleration voltage	60 kV		
Beam current	15 mA		
Wire feed speed	0.9 m/min		
Wire feed direction	side feeding, front-back feeding		
Oscillation figure			

Multitrack wall structures were selected as sample geometries, each considered three tracks wide and ten layers high. For better comparability, a wall with the dimensions 60 mm length, 5 mm width, and 12,5 mm height was determined as an idealized reference structure. In all tests, the respective layers were built up without interrupting the wire feed or the welding movement. The traveling welding path and the dimensions of the reference structure are shown in Figure 1.

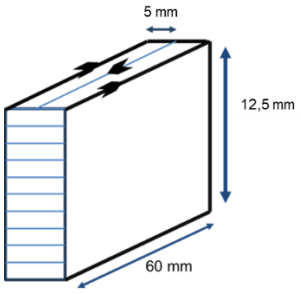

Fig. 1. Reference structure and deposition strategy of the samples.

Each layer was built up in the same direction and along the same welding path as the layer before. A complete overview of the various tests carried out and their parameters is shown in Table 4.

Table 4. Overview of the carried out tests and process parameters used.

Sample ID	Welding Speed	Wire feed direction	Oscillation figure
A	$v_w = 1\ \frac{mm}{s}$	side feeding	
B	$v_w = 1\ \frac{mm}{s}$	front-back feeding	
C	$v_w = 5\ \frac{mm}{s}$	side feeding	
D	$v_w = 5\ \frac{mm}{s}$	front-back feeding	
E	$v_w = 5\ \frac{mm}{s}$	front-back feeding	
F	$v_w = 5\ \frac{mm}{s}$	front-back feeding	
G	$v_w = 7\ \frac{mm}{s}$	front-back feeding	

For microstructure analysis, the cross-section of the as-fabricated Ti6Al4V block was cut from the midsection of the tracks using wire electric discharge machining. The samples were prepared using standard metallographic procedures. To make seams visible, the samples were polished to a surface quality of 0,1 µm and subsequently etched using Kroll's reagent for 30 seconds.

The microstructural analyses were carried out using a light optical microscope (Keyence VHX-7000, Osaka, Japan) and Zeiss Sigma 300 VP equipped with an EDS detector and an EBSD Unit. The microhardness distribution of the sample along a vertical line covering the substrate and as-deposited layers was measured using KB Prüftechnik (Hochdorf-Assenheim, Germany) Vickers hardness tester with an applied load of 500 g and a dwell time of 15 s, setting a distance of 2 mm between adjacent indentations. The chemical composition was characterized using energy dispersive x-ray spectroscopy by line scans at the base and the top of the samples to evaluate the burn-off of alloying elements during the build-up process.

3 Results and Discussion

3.1 Geometrical Accuracy

The investigation of the geometrical accuracy of the manufactured samples shows different influences of the prevailing parameters. Figure 2 illustrates the variations in the dimensions of the samples along the welding path. Since no significant local accumulation of dimensional deviations is observed, the cross-sections of the samples are analyzed to assess deviations in the height and width of the structures.

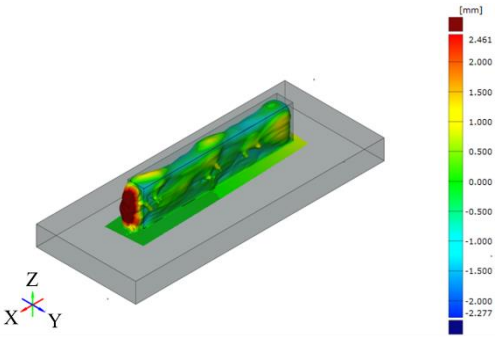

Fig. 2. Comparative representation of the created sample (F) with the idealized reference structure to show oversize and undersize.

As shown in Figure 3, one of the most critical factors influencing the height of the samples is the welding speed.

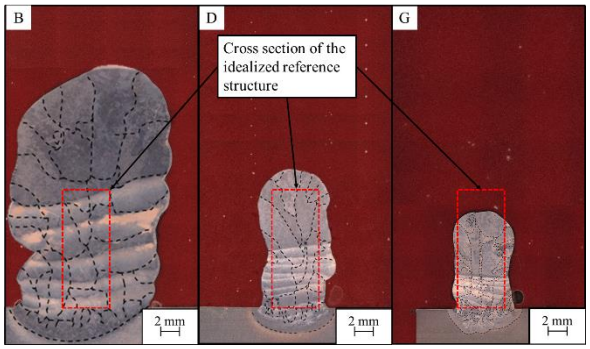

Fig. 3. Influence of the welding speed on the geometrical accuracy of the samples, the cross-section of the idealized reference structure is marked in red, the dashed black lines show the formed coarse structure.

At the same time, there is a visible difference depending on the wire feed direction. For a side wire feeding direction the manufactured components are narrower and taller than the ones manufactured by a front-back wire feeding direction, like shown in figure 4.

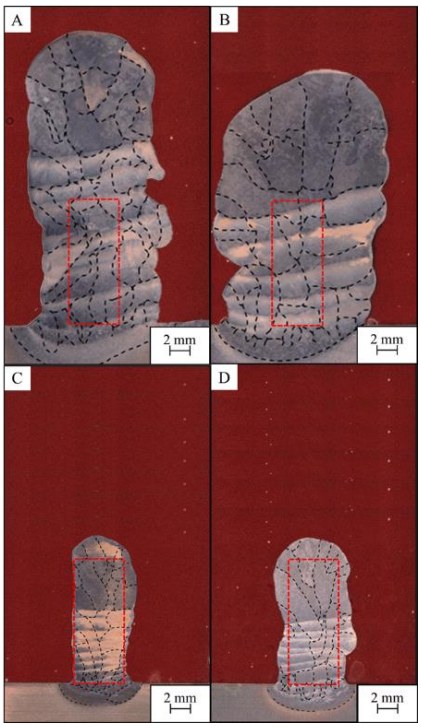

Fig. 4. Influence of the wire feed direction on the geometrical accuracy of the samples, the cross-section of the idealized reference structure is marked in red, the dashed black lines show the formed coarse structure.

In addition to these parameters, Figure 5 demonstrates a significant influence of the oscillation figure used.

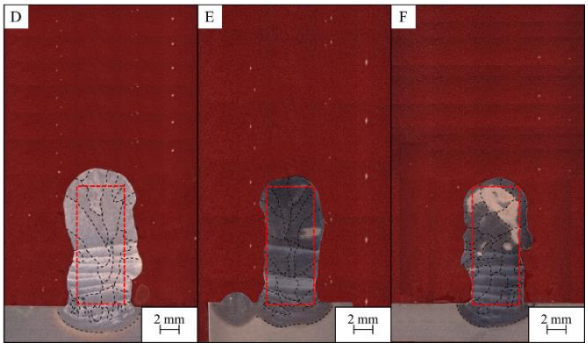

Fig. 5. Influence of the oscillation figure on the geometrical accuracy of the samples, the cross-section of the idealized reference structure is marked in red, the dashed black lines show the formed coarse structure.

As shown in Figure 5, although the oscillation patterns seem to have minimal influence on the width and height of the samples, they significantly affect the symmetry of the samples. There is a noticeable trend where more complex oscillation patterns result in increased symmetry and straightness along the building direction. Specifically, the sample constructed with a circular oscillation pattern exhibits pronounced curvatures, bulges, and indents. In contrast, the sample built with a rectangular pulse oscillation pattern shows no bulges and fewer curvatures along its build direction. Finally, the sample using a distorted infinity symbol as the oscillation pattern displays the lowest levels of curvature and bulging. The experimental findings highlight the nuanced impact of various parameters on the shape of fabricated structures, including welding

speed, wire feed direction, and the oscillation pattern employed. This corroborates earlier findings by Dragunov et al., who observed a correlation between oscillation pattern and the cross-sectional profile of single-track beads in titanium alloys [22]. Our results indicate a discernible influence of oscillation patterns on the geometric precision of multi-track structures, offering insights into customizing the assembly process for specific components. Particularly intriguing is the observation that more complex oscillation patterns tend to enhance the symmetry of built structures, presenting opportunities for refining manufacturing processes. Notably, while employing a fully symmetrical circular pattern yields less linear structures, adopting a rectangular pulse with a single symmetry axis significantly improves straightness. Further enhancement in symmetry is observed with the use of a distorted infinity symbol, likely due to its irregular energy distribution. This distribution influences the heat distribution and convection of the weld pool by increasing the energy contribution on one side of the weld pool. The resulting one-sided excess heat of the weld pool allows the wire to remain molten for a longer time and imprints a flow direction on the melt due to the heat gradient. This additional heat gradient gives the solidification of the weld pool a further direction and reduces the dependence of the solidification process on the previously deposited layers. This makes the solidification and therefore the geometric accuracy of the layers less dependent on the statistical distribution of any welding defects in the previous layers and promoting uniformity and predictability in geometric accuracy. As result of such a solidification behavior there would have to be a one-sided elevation on the highest deposited component layer, such as shown in figure 5. Petrat et al. already described that there is a significant difference in weld bead geometry according to different heat gradients depending on the deposition strategies for laser metal deposition [23]. Furthermore, Nikam et al. also showed by pre-heating that the weld pool geometry can be influenced by changes in the heat gradient [24]. This supports the assumption that a small-scale thermal gradient also influences the melt pool geometry through the oscillation figure used.

3.2 Chemical composition and Microstructure

The analysis of the chemical composition of the samples indicates a loss of alloy elements during the manufacturing process. Further measurements reveal that there is no segregation of elements, and all available elements are evenly distributed over the sample surfaces. An exemplary overview of the chemical compositions is provided in Figure 6. This figure shows a significant loss of aluminum in the buildup direction for all analyzed samples, while the concentrations of other alloying elements remain nearly constant. The aluminum loss ranges from about 1 to 1.5 weight percent relative to the chemical composition of the wire and base plate used. This reduction in aluminum content appears to be independent of the prevailing process parameters.

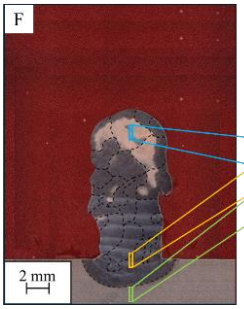

Position	Ti (wt-%)	Al (wt-%)	V (wt-%)	Fe (wt-%)
Sample top	90,8	4,8	4,1	0,3
Sample base	90,4	6,1	3,4	0,1
Base plate	89,6	6,2	4,0	0,2

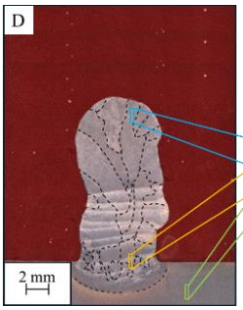

Position	Ti (wt-%)	Al (wt-%)	V (wt-%)	Fe (wt-%)
Sample top	91,1	5	3,8	0,1
Sample base	90,3	5,8	3,7	0,2
Base plate	89,6	6,2	4,0	0,2

Fig. 6. Development of the alloy composition over the samples.

The microstructure analysis of the samples, depicted in Figures 3-5, reveals a consistent presence of coarse-grained structures, characterized by grain sizes in the millimeter range. Additionally, there is evident coarsening of the structure in the building direction, accompanied by conspicuous columnar grain growth. Although the influence of the wire feed direction on grain growth appears relatively minor, it is observed that columnar grain growth tendencies are slightly more pronounced when the wire feed direction aligns with the main moving direction, as opposed to side wire feed orientation. Simultaneously, it is evident that as welding speed increases, the grain structure becomes finer, predominantly epitaxial, as depicted in Figure 3. Conversely, Figure 5 illustrates samples built with identical welding speeds but employing different oscillation figures. It becomes apparent that with more complex oscillation figures, there are recognizable changes in the microstructure along the building direction. While only minimal differences can be observed between the samples near the base plate, epitaxial growth decreases in the direction of the building. This trend is particularly prominent in sample F, where the microstructure transitions to a coarse yet nearly equiaxial grain structure in the upper third of the sample. A detailed image of the grain structure can be seen in Figure 7.

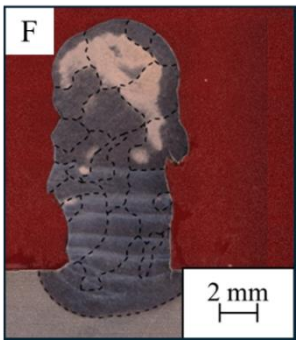

Fig. 7. Detailed view of the microstructure of sample F, the almost uniform grains in the upper third of the sample are striking.

A further examination of the microstructure of the samples shows that the large grains in the upper areas of the samples are of hexagonal α-titanium phase with almost no bcc β-titanium phase. Analyzing the chemical composition of the considered samples shows a clear loss of aluminum as reported by in literature [15,25]. The loss of slightly more than about 1 weight percent aluminum along the buildup direction is within the usual range. A possible reason for the higher loss of aluminum that Pixner et al. mentioned is the higher energy density used for fabrication of the considered samples. This suggests that the influence of the process parameters under consideration has only a minor impact on the loss of aluminum. The investigation of the microstructure of the manufactured samples shows various results. While it can be shown that a higher welding speed decreases the grain growth, at the same time the structure of columnar grain growth is not affected of a higher welding speed like Gong et al. already investigated [26]. One explanation for this is the uniaxial heat conduction in the direction of the component, which dominates the driving force of solidification. At the same time, the increase in welding speed leads to a smaller volume distribution of the weld metal and therefore faster solidification of the weld pool. A deviation from this behavior can be seen in a change of the used oscillation figures. Just like the geometrical accuracy, the microstructure seems to be significantly influenced by the used oscillation figure. Thus, with decreasing symmetry and increasing complexity of the used oscillation figure a change in the microstructure of the samples can be observed in figure 8.

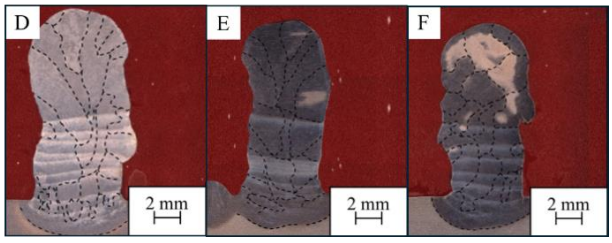

Fig. 8. Detailed view of the microstructure depending on the used oscillation figure.

The columnar grain growth is developed for the oscillation figure circle (sample D) over the whole sample. In contrast, the grain structure of the sample made with a square pulse oscillation figure is still columnar, but the grains are wider in the edge area of the sample in its upper third of the sample. At last, the sample made with a distorted infinity symbol (sample F) shows a nearly equiaxial grain structure in its upper third. A possible reason for those differences is the irregular energy input of the used oscillation figures. The distorted infinity symbol leads to a highly uneven energy input with a one-sided excess energy and heat in the weld pool, this extends the prevailing thermal gradient in the building direction by a further thermal gradient in the direction of the decreasing energy distribution of the oscillation figure. This gradient is approximately perpendicular to the buildup direction and increases the width of the forming grains such a growth in direction of the temperature gradient has already been mentioned by Gurianov et al. for titanium and nickel alloys [27]. Such an influence would only become apparent in the upper layers of the samples, as the temperature difference between the weld pool and the base plate would dominate the nucleation and solidification of the weld pool in the lower layers like Lopez-Castano et al. described [28,29]. Petrat et al. already described that there is a significant difference in weld bead geometry according to different heat gradients depending on the deposition strategies for laser metal deposition. This supports the assumption that a small-scale thermal gradient also influences the melt pool geometry through the oscillation figure used [23].

3.3 Hardness tests

The results of the microhardness tests indicate comparable results across all samples, showcasing an almost uniform microhardness distribution throughout their entire cross-sectional surfaces. It is noteworthy that the hardness values of the samples are consistently lower than those of the base plates. Notably, no significant disparities in hardness values are observed among the samples, irrespective of the varied process parameters employed. For illustrative purposes, Figure 9 provides a representative hardness distribution.

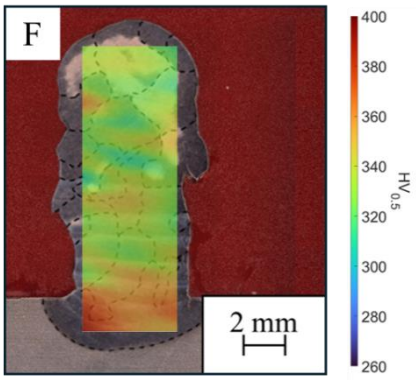

Fig. 9. Hardness distribution over the cross-section of the manufactured samples.

4 Conclusions

The results of the investigations carried out show that in addition to welding speed and wire feed direction also the used oscillation figure during the EBAM has a visible influence on both geometric accuracy and microstructure of the manufactured samples. The usage of a less symmetric energy input on the samples seems to increase equiaxial grain growth in higher areas of the sample. As well the less symmetric energy input seems to make a straighter buildup and better geometrical accuracy of the samples possible and enables to reduce the material oversize for a subsequent mechanical processing.

References

1. Frazier, William E. (2014): Metal Additive Manufacturing: A Review. In: *J. of Materi Eng and Perform* 23 (6), P. 1917–1928
2. Moghimian, Pouya; Poirié, Thomas; Habibnejad-Korayem, Mahdi; Zavala, Javier Arreguin; Kroeger, Jens; Marion, Frédéric; Larouche, Frédéric (2021): Metal powders in additive manufacturing: A review on reusability and recyclability of common titanium, nickel and aluminum alloys. In: *Additive Manufacturing* 43, P. 102017
3. Herzog, Dirk; Seyda, Vanessa; Wycisk, Eric; Emmelmann, Claus (2016): Additive manufacturing of metals. In: *Acta Materialia* 117, P. 371–392
4. Michel, Florent; Lockett, Helen; Ding, Jialuo; Martina, Filomeno; Marinelli, Gianrocco; Williams, Stewart (2019): A modular path planning solution for Wire + Arc Additive Manufacturing. In: *Robotics and Computer-Integrated Manufacturing* 60, P. 1–11
5. Taminger, Karen M. B.; Hafley, Robert A. (2003): Electron Beam Freeform Fabrication: A Rapid Metal Deposition Process. In:. 3rd Annual Automotive Composites Conference
6. Zhai, Yuwei; Lados, Diana A.; LaGoy, Jane L. (2014): Additive Manufacturing: Making Imagination the Major Limitation. In: *JOM* 66 (5), P. 808–816
7. Taminger, Karen M.; Hafley, Robert A. (2006): Electron Beam Freeform Fabrication for Cost Effective Near-Net Shape Manufacturing. In:. NATO/RTO AVT-139 Specialists" Meeting on Cost Effective Manufacture via Net Shape Processing
8. Schultz, Helmut (2017): Elektronenstrahlschweißen. Grundlagen, Maschinen und Anwendungen. 3., vollständig überarbeitete und erweiterte Auflage. Düsseldorf: DVS Media (Fachbuchreihe Schweißtechnik, Band 93)
9. Reisgen, Uwe; Gach, Stefan (2021): Electron beam welding. In: Advanced Joining Processes: Elsevier, P. 35–65
10. Liu, Yongjie; Liu, Fulin; He, Ruixiang; Wang, Qingyuan; Wang, Chong; He, Chao et al. (2021b): Mechanical behaviors of electron beam welded titanium alloy up to very high cycle fatigue under different process conditions. In: *Materials Science and Engineering: A* 802, P. 140685
11. Abdulhameed, Osama; Al-Ahmari, Abdulrahman; Ameen, Wadea; Mian, Syed Hammad (2019): Additive manufacturing: Challenges, trends, and applications. In: *Advances in Mechanical Engineering* 11
12. Wanjara, P.; Watanabe, K.; Formanoir, C. de; Yang, Q.; Bescond, C.; Godet, S. et al. (2019): Titanium Alloy Repair with Wire-Feed Electron Beam Additive Manufacturing Technology. In: *Advances in Materials Science and Engineering* 2019, P. 1–23
13. Zhang, Lai-Chang; Liu, Yujing; Li, Shujun; Hao, Yulin (2018): Additive Manufacturing of Titanium Alloys by Electron Beam Melting: A Review. In: *Adv Eng Mater* 20 (5), Artikel 1700842
14. Körner, C. (2016): Additive manufacturing of metallic components by selective electron beam melting — a review. In: *International Materials Reviews* 61 (5), P. 361–377
15. Xu, Junqiang; Zhu, Jun; Fan, Jikang; Zhou, Qi; Peng, Yong; Guo, Shun (2019): Microstructure and mechanical properties of Ti–6Al–4V alloy fabricated using electron beam freeform fabrication. In: *Vacuum* 167, P. 364–373
16. Greitemeier, Daniel (Hg.) (2016): Untersuchung der Einflussparameter auf die mechanischen Eigenschaften von additiv gefertigtem TiAl6V4. Wiesbaden: Springer Vieweg
17. Liu, Guo; Zhang, Xiaofeng; Chen, Xuliang; He, Yunhu; Cheng, Lizi; Huo, Mengke et al. (2021a): Additive manufacturing of structural materials. In: *Materials Science and Engineering: R: Reports* 145, P. 100596
18. Fuchs, J.; Schneider, C.; Enzinger, N. (2018): Wire-based additive manufacturing using an electron beam as heat source. In: *Weld World* 62 (2), P. 267–275
19. Pixner, Florian; Warchomicka, Fernando; Peter, Patrick; Steuwer, Axel; Colliander, Magnus Hörnqvist; Pederson, Robert; Enzinger, Norbert (2020): Wire-Based Additive Manufacturing of Ti-6Al-4V Using Electron Beam Technique. In: *Materials (Basel, Switzerland)* 13 (15)
20. Klimenov VA, Fedorov V V., Slobodyan MS, Pushilina NS, Strelkova IL, Klopotov AA, et al. Microstructure and Compressive Behavior of Ti-6Al4V Alloy Built by Electron Beam Free-Form Fabrication. J Mater Eng Perform 2020;29:7710–21
21. Gudenko A V., Sliva AP Influence of electron beam oscillation parameters on the formation of details by electron beam metal wire deposition method. J Phys Conf Ser 2018;1109
22. Dragunov, V. K.; Goryachkina, M. V.; Gudenko, A. V.; Sliva, A. P.; Shcherbakov, A. V. (2019): Investigation of the optimal modes of electron-beam wire deposition
23. Petrat, Torsten; Winterkorn, René; Graf, Benjamin; Gumenyuk, Andrey; Rethmeier, Michael (2018): Build-up strategies for temperature control using laser metal deposition for additive manufacturing. In: *Weld World* 62 (5), S. 1073–1081
24. Nikam, Sagar H.; Jain, Neelesh K. (2018): Finite Element Simulation of Pre-Heating Effect on Melt Pool Size During Micro-Plasma Transferred Arc Deposition Process. In: *IOP Conf. Ser.: Mater. Sci. Eng.* 389 (1), P. 12006
25. Pixner, Florian; Buzolin, Ricardo; Warchomicka, Fernando; Pilz, Andreas; Enzinger, Norbert (2022): Wire-based electron beam additive manufacturing of tungsten. In:

International Journal of Refractory Metals and Hard Materials 108, S. 105917

26. Gong, Xibing; Lydon, James; Cooper, Kenneth; Chou, Kevin (2014): Beam speed effects on Ti–6Al–4V microstructures in electron beam additive manufacturing. In: *J. Mater. Res.* 29 (17), P. 1951–1959
27. Gurianov, D. A.; Kalashnikov, K. N.; Utyaganova, V.; Khoroshko, E. S.; Chumaevskii, A. V. (2019): Microstructure features of Ni-based and Ti-based alloys formed by method of wire-feed electron beam additive technology. In: *IOP Conf. Ser.: Mater. Sci. Eng.* 597 (1), P. 12042
28. Lopez-Castaño, Silvia; Emile, Philippe; Archambeau, Claude; Pettinari-Sturmel, Florence; Douin, Joël (2021): Main Microstructural Characteristics of Ti-6Al-4V Components Produced via Electron Beam Additive Manufacturing (EBAM). In: *TMS 2021 150th Annual Meeting & Exhibition Supplemental Proceedings*, P. 176–188
29. Ding, Xiao; Koizumi, Yuichiro; Wei, Daixiu; Chiba, Akihiko (2019): Effect of process parameters on melt pool geometry and microstructure development for electron beam melting of IN718: A systematic single bead analysis study. In: *Additive Manufacturing* 26, P. 215–226+